ANALYSIS OF POLARIMETRIC BISTATIC SEA CLUTTER USING THE NETRAD RADAR SYSTEM

Francesco Fioranelli[(1)], Matthew Ritchie[(1)], Hugh Griffiths[(1)], Stephan Sandenbergh[(2)], Michael Inggs[(2)]

[(1)]Department of Electronic and Electrical Engineering, University College London, WC1E 7JE, London, UK
[(2)]Department of Electrical Engineering, University of Cape Town, 7701, Rondebosch, South Africa

Abstract

This paper presents a comparative analysis of amplitude and Doppler spectra statistics from monostatic and bistatic sea clutter data at S-band. These data cover a range of bistatic angles from 60° to 120° and include simultaneous monostatic and co-polarized and cross-polarized bistatic recordings, providing direct comparison of their statistical properties. The time series of amplitude data are fitted to the compound K and K+Noise distribution in the range domain and in the Doppler domain, and the variation of the shape parameter is presented for monostatic and co-polarized and cross-polarized bistatic data as an indication of the spikiness of the clutter. From the analysis of this parameter it is shown that cross-polarized bistatic data tend to be less spiky in the range and Doppler domain than the simultaneous co-polarized bistatic data, and than the simultaneous monostatic data, which could be advantageous in terms of radar detection performance, especially for low-visibility maritime targets.

1. Introduction

There is growing interest in the use of bistatic and multistatic radar for the detection, tracking, and classification of small low-visibility maritime targets, such as small boats and inflatables that may be used in smuggling and trafficking, as well as for supporting search and rescue operations. Bistatic and multistatic radar may offer potential advantages over conventional monostatic radar, such as enhanced target signatures and improved detection using multi-perspective views, and the fact that the receive-only passive nodes are less complex and more compact, hence suitable to be mounted on UAVs or other unmanned platforms for enhanced surveillance operations. A comprehensive knowledge of the behaviour of bistatic clutter is however necessary to fully understand and characterize these potential advantages over conventional monostatic architectures, as the clutter statistics affect the design and optimization of detection algorithms and the overall radar performance. Openly published information on bistatic clutter is currently limited for a series of reasons, including the fact that the necessary measurements are complex to conduct and the results depend on many variables. A good summary of previous work on bistatic clutter measurements can be found in chapter 9 by Weiner [1], which lists nine programmes of measurements, with only four covering sea clutter. Previous work on the characterization of bistatic sea clutter has been presented within the collaboration between University College London (UCL) and the University of Cape Town (UCT) to collect and analyse data on multistatic sea clutter and maritime targets, using the netted radar system NetRAD [2]. These data

have provided significant results for the characterization of bistatic sea clutter radar cross section [3], amplitude statistics [4], and Doppler spectra [5, 6], and highlighted the potential advantageous properties of sea clutter in bistatic geometries, in particular the reduced effects of spike events in the amplitude and Doppler domain comparing simultaneous monostatic with bistatic data. The data analysed in these papers were collected in October 2010 and included different bistatic angles (15°, 30°, 60°, 90°, and 120°) and VV and HH co-polarized measurements, plus a single cross-polarized measurement reported in [3, 4].

The work presented in this paper aims at expanding the knowledge of bistatic clutter through the analysis of additional NetRAD data collected in a different experimental campaign in June 2011, which has never been published in the previous literature. It is believed that these datasets contain significant elements of novelty, which can help provide a better understanding of clutter diversity, i.e. the variation of sea clutter features over numerous parameters such as bistatic geometry, sea state, polarization, as well as many others. The main element of novelty is the fact that three radar nodes were simultaneously used rather than only two, and this allowed the simultaneous recording of bistatic data in both co-polarized and cross-polarized components with respect to the polarization transmitted by the monostatic node. This provides a direct comparison of simultaneous co-polarized and cross-polarized bistatic clutter characteristics, as well as the comparison with the monostatic clutter simultaneously recorded at the transceiver node. It is therefore believed that the analysis presented within this work contributes novel quantitative information on bistatic sea clutter. A unique aspect of the data analysed is that for each transmitted and received polarization combination, the data were collected over a relatively short amount of time at seven different bistatic angles from 60° to 120°. This allows a smoother analysis of clutter characteristics and trends as a function of bistatic angle for each polarization compared to previous dataset analysis [3-4, 6-7], where the slow evolution of sea parameters might have had an effect. Some of the measurements programmes on bistatic clutter discussed in chapter 9 of [1] recorded simultaneous co-polarized and cross-polarized bistatic data, such as in [8] by Pidgeon at C-band and in [9] by Kochanski at X-band, but there is no clear reference to simultaneous monostatic clutter data for a proper comparison. A more detailed discussion on the novelty of bistatic NetRAD data with respect to these previous works can be found in chapter 2 of [10].

Additional information on the radar system, the experimental setup, and the dataset is presented in section 2 of this paper. Section 3 presents the analysis of the data, focusing on the characterization of clutter amplitude statistics and Doppler spectra using the shape parameter of the compound K and K+Noise distribution to evaluate the spikiness of the clutter. The analysis compares monostatic with simultaneous bistatic data, as well as simultaneous co-polarized with cross-polarized bistatic data. It is shown that bistatic clutter is characterized by less spiky distribution which may be beneficial to improve the radar detection performance, and that cross-polarized bistatic clutter is even less spiky than the simultaneous co-polarized. Finally section 4 concludes the paper discussing potential future work on the data and on the development of the successor system of NetRAD, NeXtRAD.

2. Radar System and Data Collection

The system used to collect the data in this paper is the pulse coherent multistatic radar NetRAD, which consists of three distinct but essentially identical radar nodes. The system was developed at UCL over the past few years and was modified in collaboration with UCT to be suitable to collect sea clutter data with different nodes separated by baselines of the order of kilometres, as detailed in [10-11]. The radar parameters for the data analysed here were 2.4 GHz frequency, 45 MHz linear up-chirp bandwidth, 1 kHz Pulse Repetition Frequency (PRF), 130000 pulses equal to 130 seconds per recording, and pulse length between 1.8 μs and 3 μs depending on the geometry. The peak transmitted power was 450 W. Only one high power transmitter was used during the experiment, whereas the additional radar nodes were used as passive receivers. The antenna used had approximately 24 dBi gain and 10° x 10° beam-width in azimuth and elevation. The data were collected on June 9 2011 in South Africa at Misty Cliffs near the village of Scarborough and facing the Atlantic Ocean on the west side of the Cape Peninsula. Figure 1 shows a map of the experiment location, with a baseline of approximately 1830 m between the monostatic transceiver node (node 3) and the two co-located bistatic receiver nodes (node 1 and node 2). The nodes were synchronized and triggered using the GPS Disciplined Oscillators (GPSDOs) developed at the University of Cape Town (UCT) and described in [11-12]. The GPSDOs provided also the coordinates and altitudes of the nodes, and the resulting grazing angle varied between 0.7° and 1.12° with the different bistatic angles. This is considered very low grazing angles, and is below the critical angle (approximately 10° depending on sea state) where the RCS values reduce significantly and the amplitude statistics exhibit particularly non-Gaussian behaviour.

Table 1 presents the list of the 21 datasets analysed in this paper, indicating the value of bistatic angle, the polarization at each node, and the extension of the analysed clutter patch (reported as the length of the area where the transmitter and receiver antenna patterns intersect, with two examples shown in figure 1 for the smallest and largest bistatic angles). Node 1 always received H polarization and node 2 V polarization, whereas the transmitted and received polarizations at node 3 were changed during the day. Figure 1 shows also the direction pointed by the antennas when collecting data at the largest and smallest bistatic angles, respectively 120° and 60°. The antennas were manually rotated and pointed to a common clutter patch using optical telescopic sights and turntables with precision mechanical azimuth readouts, while stepping through the various bistatic angles during the experiment. The use of such sights plus a Vernier scale provided precision capability up to 0.2° (1/50 beamwidth).The available wind and wave data recorded on the day shows a wind speed of approximately 8-9 m/s blowing from the South-South-East direction, and wave height of approximately 2 m (estimated sea state 4) and direction approximately 225° with respect to True North, with these conditions remaining constant during the experiment.

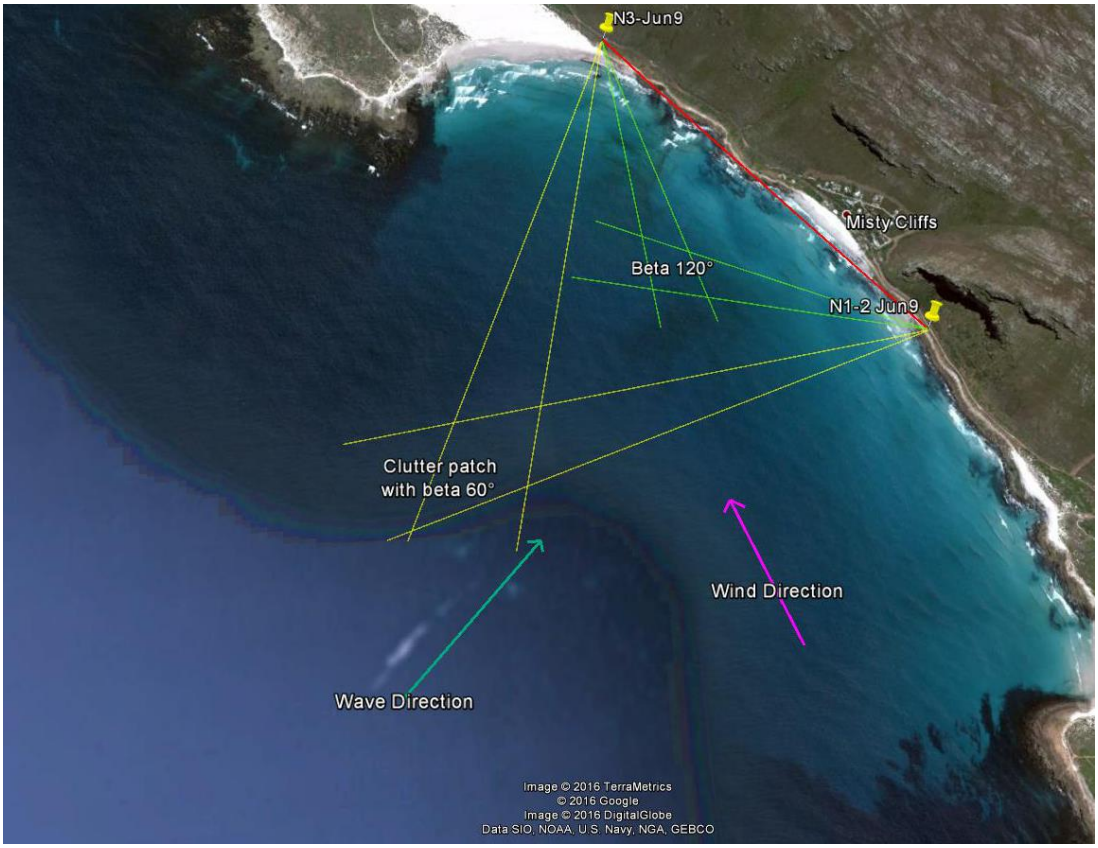

Figure 1 Experimental location with two bistatic angles as example

Table 1 Summary of the datasets with bistatic angle and polarization

Dataset number	Node 3 Polarization (Tx-Rx)	Node 1 Polarization (Rx)	Node 2 Polarization (Rx)	Bistatic Angle [°]	Clutter Patch Limits [m]
1	HH	H	V	60	300
2	HH	H	V	75	300
3	HH	H	V	85	240
4	HH	H	V	90	210
5	HH	H	V	95	210
6	HH	H	V	105	180
7	HH	H	V	120	120
8	VH	H	V	60	300
9	VH	H	V	75	300
10	VH	H	V	85	240
11	VH	H	V	90	210
12	VH	H	V	95	210
13	VH	H	V	105	180
14	VH	H	V	120	120
15	VV	H	V	60	300
16	VV	H	V	75	300
17	VV	H	V	85	240
18	VV	H	V	90	240
19	VV	H	V	95	210
20	VV	H	V	105	180
21	VV	H	V	120	120

3. Data Analysis

3.1 Analysis of Amplitude Statistics

The K distribution was initially proposed by Jakeman and Pusey [13] and is a well-established model to represent sea clutter amplitude statistics for high resolution radar at low grazing angles. A compound version of the distribution was also proposed in [14] and discussed in chapters 2-3 of [15]. This formulation allows to characterise two different components contributing to the clutter amplitude fluctuations and to describe both amplitude and correlation properties. The first component is a spatially varying mean level associated to long sea waves and swell structure, with slow temporal variation and long correlation time. The second component is the local speckle related to small capillary waves and local interactions between sea water and winds, with faster variations and much shorter correlation time. The speckle intensity component can be modelled with a negative exponential distribution, with its mean value modulated by a Gamma distribution [15]. Hence the probability density function (PDF) of the K distribution intensity is described by equation (1), where b is the amplitude scale parameter, ν is the shape parameter, Γ is the gamma function, and $K_{\nu-1}$ is the modified Bessel function of the second kind and order ν-1.

$$P(z) = \frac{2b^{\frac{\nu+1}{2}} z^{\frac{\nu-1}{2}}}{\Gamma(\nu)} K_{\nu-1}(2\sqrt{bz}) \tag{1}$$

Additional distributions have been proposed to model amplitude statistics of non-Gaussian sea clutter, among which log-normal [16], Weibull [17], generalized gamma texture model [18], and generalized Pareto in [19, 20] and in [21] where the multidimensional complex Pareto distribution is derived as a specific case of the compound Gaussian family to model clutter distributions whose tails are heavier than any K distribution. Extensions of the K distribution mentioned above have been also presented to take into account the thermal noise of the radar (K+Noise distribution [15, 22, 23]), to improve the model of the presence of discrete spiking events (KA distribution [24, 25]), and to fit more precisely the tail of the distribution using two discrete K distributions (KK distribution [26]). A comparative analysis of fitting five different distributions to bistatic clutter data can be found in [4], where the KA was reported to provide the best fit for most of the datasets. A detailed analysis of experimental sea clutter data collected by the monostatic X-band McMaster University IPIX radar has been presented in [23], where the validity of non-Gaussian clutter models using K and K+Noise distributions has been demonstrated for data related to coastal waters at relatively short ranges. Reference [27] has also discussed the suitability of bi-parametric family of distributions, in particular Weibull and K distributions, to characterize first-order amplitude statistics of low grazing angle and high resolution sea clutter, using experimental data collected by the same McMaster University radar system. The PDF of the K+Noise distribution is reported in equation (2), where x is the local clutter intensity, P_N is the receiver noise power, ν is the shape parameter, and b is the amplitude scale parameter.

$$P(z) = \frac{b^{\nu}}{\Gamma(\nu)} \int_0^{\infty} x^{\nu-1} \frac{\exp(-bx)}{x+p_N} \exp\left(\frac{-z}{x+p_N}\right) dx \quad (2)$$

In this paper we want to fit the data to the K and/or K+Noise distribution and analyse the shape parameter *v* as a function of bistatic angle and polarization. This parameter is linked to the level of spikiness of the clutter, where "spiky" refers to data presenting a significant number of isolated strong returns in individual range bins, which typically refer to whitecaps and other non-Bragg scattering events [15]. The spikiness of the clutter has also an impact on the radar detection performance, as spiky clutter has longer tail in its PDF and in general reduces the probability of detection and the detection threshold for a given probability of false alarm, providing poorer detection sensitivity. This is not always true, as it has been shown that for low probability of detection the opposite case can happen [28]. Values of the shape parameter for sea clutter are generally in the range from 0.1 to infinity. The distribution of the clutter tend to become more and more Rayleigh-distributed with increasing values of the shape parameter *v*, whereas small values in the range *v* smaller than 1 are associated with spiky clutter [15].

The first step of the analysis was the identification of the clutter patch common to the monostatic and bistatic nodes in the Range Time Intensity (RTI) plots from the data recorded at each node. Figure 2 shows an example of these plots for the dataset 3, corresponding to 85° bistatic angle, where the typical waves structure of sea clutter can be seen. The two-way range used to compare monostatic and bistatic data is defined as the transmitter-to-target range plus the target-to-receiver range. The figures have been normalized to the peak level within each plot.

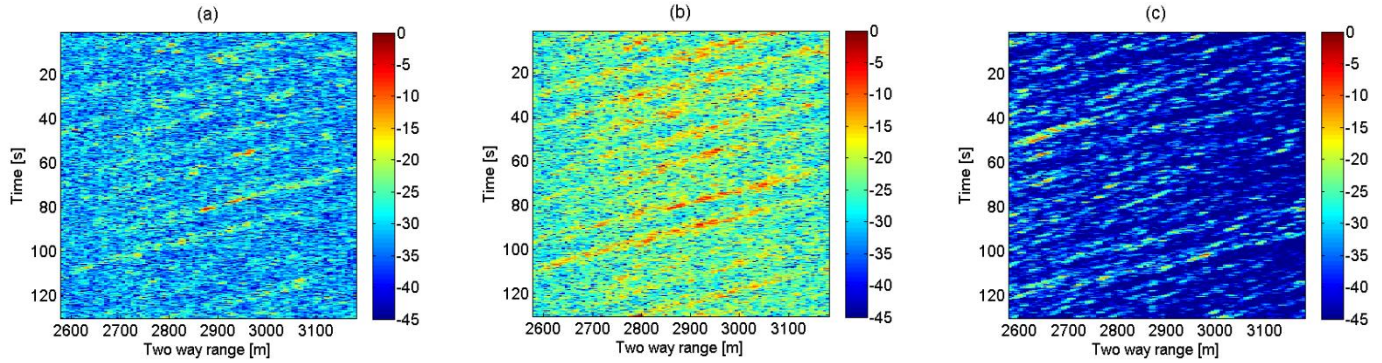

Figure 2 Example of simultaneous RTI clutter patches from dataset 3 with β equal to 85°: (a) Bistatic node 1 HH pol, (b) Bistatic node 2 HV pol, and (c) Monostatic node 3 HH pol

The time series of intensity samples at each range bin can be statistically characterised by estimating the shape parameter *v* of the K or K+Noise distribution. In our case for each range bin the time series is made of 130,000 samples, corresponding to a recorded duration of 130 s at 1 kHz PRF.

Several methods have been proposed in the literature to estimate the shape parameter of the K distribution. A first approach uses the relation between the second normalised moment of the time series and the shape parameter *v*, as indicated in chapters 6 and 13 of [15] and in [23], and used for instance in [5-6]. The formula is reported in equation (3). Another approach is based on the estimates of the mean of the data and of the

mean of the logarithm of the data, as discussed in chapter 13 of [15] and in [29-31], and reported in equation (4) where N is the number of non-coherently integrated pulses.

$$\frac{\langle z^2 \rangle}{\langle z \rangle^2} = 2\left(1 + \frac{1}{\tilde{\nu}}\right) \tag{3}$$

$$\frac{\langle z\, logz \rangle}{\langle z \rangle} - \langle z\, logz \rangle - \frac{1}{N} = \frac{1}{\tilde{\nu}} \tag{4}$$

Another approach calculates the complementary cumulative distribution function (CCDF) from the actual data samples, and fits this function to a series of theoretical CCDF K-distribution curves with different shape parameters to find the best fit. The mean square error in the log domain between the experimental and theoretical curves is calculated for each theoretical curve, and the curve that minimizes such error is selected as best fit to the data and its shape parameter is recorded. The theoretical CCDF curves are generated according to equation (5), which refers to a linear detector without including the radar system noise. In this equation v is the shape parameter, a is the power threshold level, Γ is a gamma function, and K_v is a modified Bessel function of the second kind and order v.

$$F(a) = \frac{2}{\Gamma(v)}(av)^{\frac{v}{2}}\ K_v\left(2\sqrt{av}\right) \tag{5}$$

Several methods to estimate the shape parameter for the K+Noise distribution have also been proposed in the literature. The estimator based on the mean of the logarithm of the data in equation (4) has been extended to take into account the effect of thermal noise, either proposing suitable numerical methods to obtain a value of the shape parameter [31], or developing a closed-form of the estimator when more than a single pulse are non-coherently integrated together [29]. Moment matching approach has been also used, for instance estimating the second, fourth, and sixth moment as in [23], or exploiting the knowledge of the noise power P_N as in equation (6), where the first and second moment of the intensity of the clutter plus noise data are used, as reported in chapter 5 and 13 of [15] and in [22, 31].

$$\tilde{\nu} = \frac{2(\langle Z \rangle - P_N)^2}{\langle Z^2 \rangle - 2\langle Z \rangle^2} \tag{6}$$

In this paper we initially evaluated the goodness of fit of K and K+Noise distribution to the data. The shape parameter of the K distribution was estimated through fitting the CCDF of the intensity of the data (linear detector) to the theoretical curve in equation (5). The range of shape parameter values to generate the theoretical K distribution CCDF varies between 0.1 and 15 in steps of 0.01. Values of shape parameter above 15 have not been considered as these shape parameter can be assumed to be representative of a Rayleigh distribution rather than K distribution. The shape parameter of the K+Noise was estimated using equation (6). The noise power P_N was estimated from range bins in the Range-Time-Intensity plots where there is no clutter or other signals present (noise limited range bins). Figure 3 shows examples of fittings of the CCDF

of data with K and K+Noise distributions for two datasets, namely HH polarised bistatic data from dataset 3 in figure 3a and VV polarised bistatic data from dataset 17 in figure 3b. It can be empirically seen that the K+Noise provides a better fit to the data, especially in the tail region of the distribution. The goodness of fit, especially in the tail region, can be evaluated using the mean square error between data and theoretical curves in the logarithmic domain as a metric [4]. Other hypothesis methods such as the Kolmogorov-Smirnov test are not suitable as they give the same importance on all regions of the distributions under test. To provide an example of this goodness of fit metric, the mean square error between the data CCDF and the K and K+noise theoretical curves in the log domain has been evaluated for each range bin of the clutter patch of HH polarised data from dataset 3. The error in case of fitting the K distribution appears to be approximately 4 times larger than when fitting the K+Noise distribution (error equal approximately to 186 for the K distribution, and to 50 for the K+Noise), considering an average over 100 range bins.

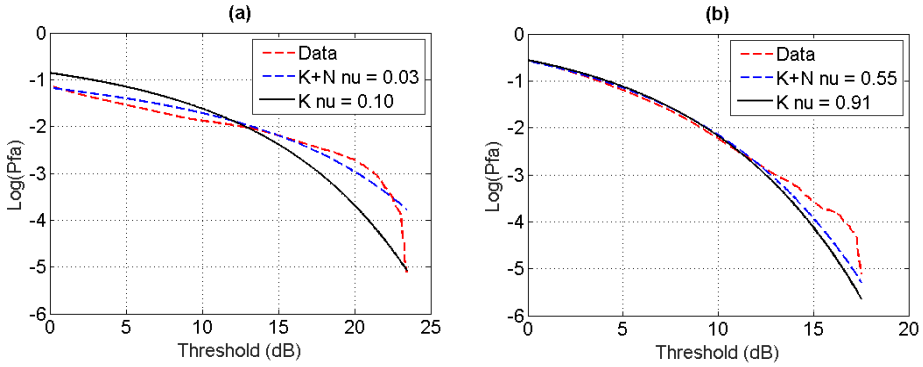

Figure 3 Examples of K and K+Noise distribution fitting to the CCDF of data: (a) HH bistatic polarised data (dataset 3), and (b) VV bistatic polarised data (dataset 17)

In the rest of this section, K+Noise distributions are fitted to the data and the shape parameters analysed to evaluate the spikiness of the clutter. As an example of results, figure 4 show examples of K+Noise distribution shape parameters for different polarizations and for bistatic angle equal to 85°. A shape parameter value was estimated for each single range bin using 130,000 samples. The results are plotted as a function of range bins, showing 20 range bins in the middle of the clutter patch. The shape parameter tends to be lower for monostatic data in comparison with both co-polarized and cross-polarized bistatic data for transmitted vertical polarization (figures 4b and 4c), whereas the values are more similar between monostatic and co-polarised bistatic and higher for cross-polarised bistatic for transmitted horizontal polarisation (figure 4a).

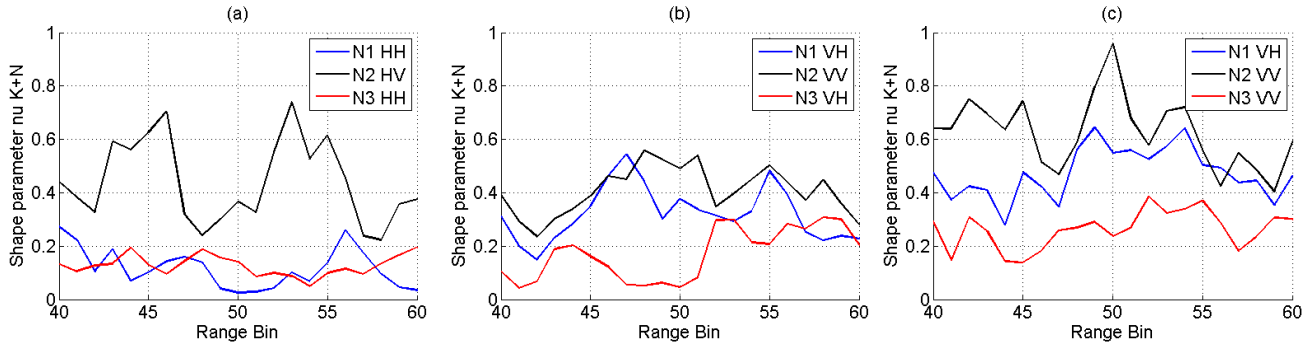

Figure 4 K+Noise distribution shape parameter as function of range bin: (a) dataset 3 β=85°, (b) dataset 10 β=85°, and (c) dataset 17 β=85°

Results in terms of K+Noise shape parameter as a function of bistatic angles for all the considered datasets and polarisations are shown in figure 5. The value of the shape parameter refers to the range bin in the middle of the clutter patch at the intersection of the transmitter and receiver beams. Previous analysis of other NetRAD data in [4, 7, 32] have commented on the fact that the sea clutter statistics appear less spiky in bistatic data compared with simultaneous monostatic data. This was also confirmed with the recent results presented in [33, 34], where simultaneous monostatic and bistatic NetRAD data were compared analysing the spikiness through the characterization of the shape parameter of the K+Noise distribution and other distributions. The analysis of these data allows to comment further on trends comparing simultaneous monostatic vs co-polarised and cross-polarised bistatic for a larger variety of bistatic angles. The shape parameter for monostatic data appears to be in general lower than for cross-polarised bistatic data. For monostatic vs co-polarised bistatic data, different results can be seen depending on polarisation and bistatic angle. For HH polarisation (figure 5a) the shape parameters appear to be very similar, with values below 0.2 in both cases. For VH and VV polarisation, the shape parameter for the monostatic data appears to be lower than for the simultaneous co-polarised data at large bistatic angles, above 90-95°, and lower for smaller bistatic angles in the range of 60-80°. Changes in bistatic angles imply also changes in range, i.e. decreasing range with increasing bistatic angle. Other works in the literature have shown that the shape parameter appears to decrease with decreasing range, at least for monostatic clutter, but this trend is not observed in these data, perhaps because the changes in range and in grazing angle are not significant enough in the given geometry.

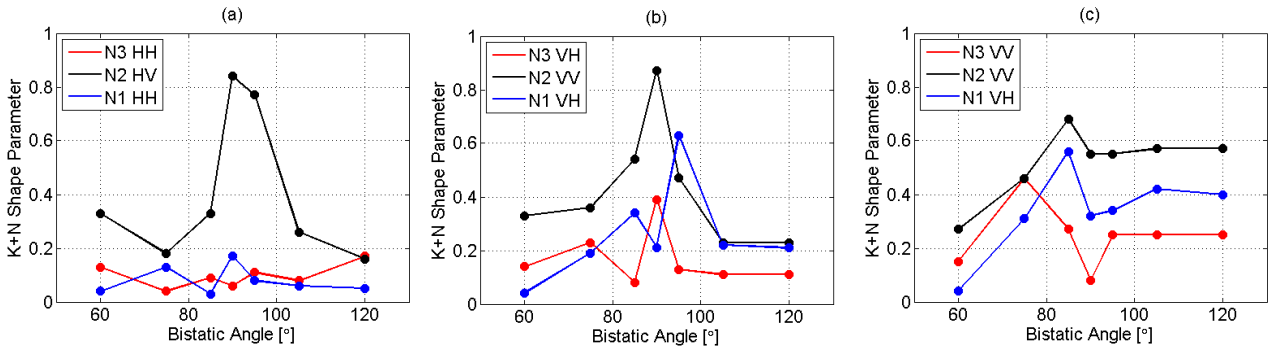

Figure 5 K+Noise distribution shape parameter for the range bin in the middle of the clutter patch as function of bistatic angle: (a) datasets 1-7, (b) datasets 8-14, and (c) datasets 15-21

Individual spikes were also isolated from the clutter background in order to gain further understanding of their presence in these clutter data. Different techniques have been proposed in the literature to isolate spikes through suitable thresholds on the data, as reported in [35]. We used the approach followed in [35, 36], with the threshold on the data set equal to $\mu+n\sigma$, where μ and σ are the mean and standard deviation of the clutter background, and n is a positive number (set equal to 5 in [35] and equal to 2 in [36]). Figures 6a-6c shows the normalized time history of the clutter samples at the range bin in the middle of the clutter patch for dataset 3. It appears that the HH monostatic data present more spike events than the corresponding HH bistatic data,

and that the simultaneous VH bistatic data present spikes as well, but with reduced intensity related to the mean intensity. Figures 6d-6f shows a similar comparison for data collected at 14.57 with VV polarized monostatic data.

The number of detected spikes events according to the aforementioned threshold criterion was counted for the clutter patch in each dataset and some results are presented in Fig. 7 as percentage of spike detection related to the overall number of clutter samples. These are plotted as a function of bistatic angles in separate figures for datasets collected with different polarizations. Two values of the parameter *n* in the threshold criterion have been chosen, namely 2 used in [35] in Fig. 7a-7c and 5 used in [36] in Fig. 7d-7f. Given the value of *n*, it would appear that in general the percentage of spike events is higher for bistatic data collected with the same polarizations as the monostatic data such as HH node 1 data vs HH node 3 data (first seven datasets in Fig. 7a and 7d). Comparing simultaneous V and H polarized bistatic data, it would appear that when H pol is transmitted the corresponding bistatic co-polarized H data has lower percentage of spikes (node 1 data vs node 2 data for first seven experiments in Fig. 7a and 7d), whereas when V pol is transmitted the corresponding bistatic co-polarised V data has higher percentage of spikes (node 2 data vs node 1 data for the other fourteen experiments in Figures 7b-7c and 7e-7f). Similar results have been obtained for values of *n* equal to 3 and 4, not reported here for space limitations. The results shown in Figure 7 were obtained just by counting the spike events using a simple intensity threshold, without investigating other characteristics of the spike events such as duration and interval between spikes as in [37], or linking spike characteristics to parameters of amplitude and Doppler statistics to distinguish between different scattering mechanisms as in [35]. A more advanced analysis of spike events goes beyond the scope of this paper and will be covered in future work.

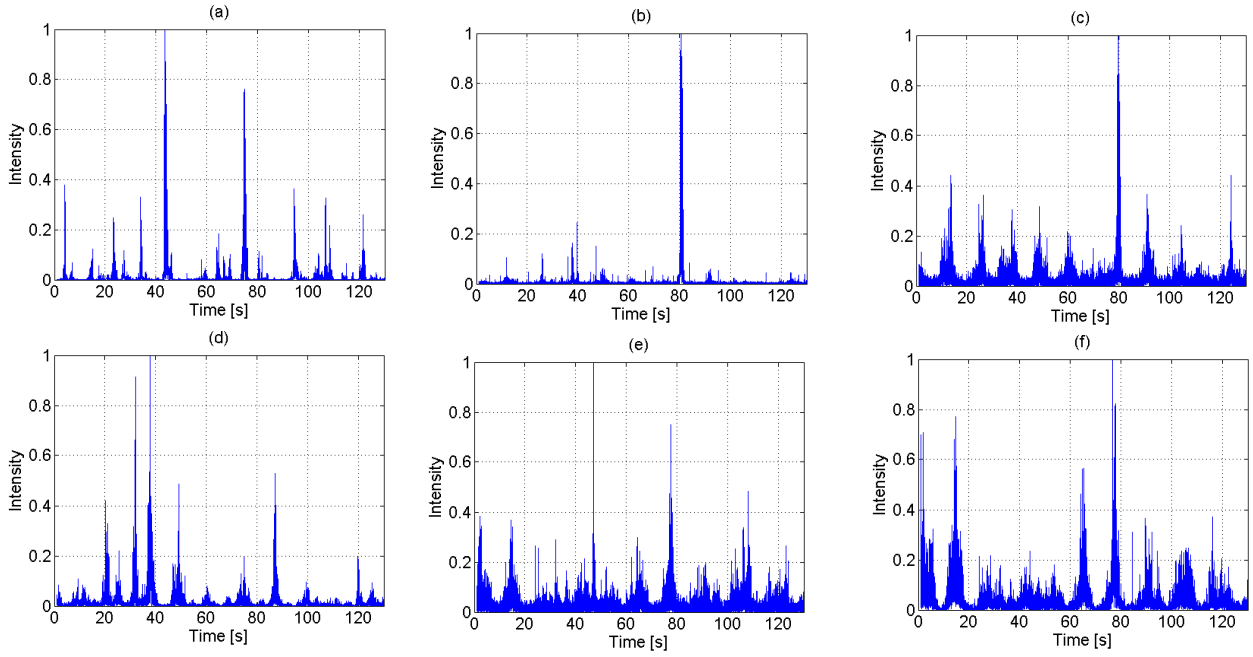

Figure 6 Time history of the data collected at different polarizations: (a) monostatic node 3 HH pol dataset 3, (b) bistatic node 1 HH pol dataset 3, (c) bistatic node 2 HV pol dataset 3, (d) monostatic node 3 VV pol dataset 17, (e) bistatic node 1 VH pol dataset 17, and (f) bistatic node 2 VV pol dataset 17

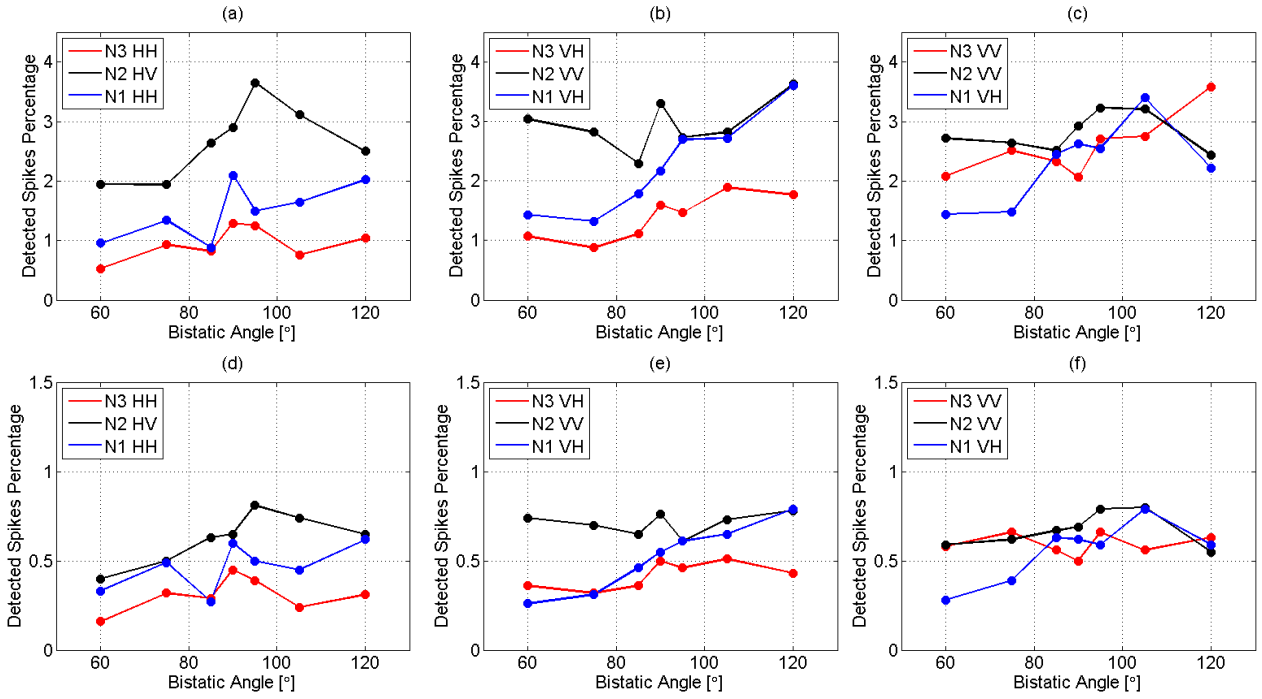

Figure 7 Percentage of spike detection as a function of bistatic angle: (a) datasets 1-7 with threshold n=2, (b) datasets 8-14 with threshold n=2, (c) datasets 15-21 with threshold n=2, (d) datasets 1-7 with threshold n=5, (e) datasets 8-14 with threshold n=5, and (f) datasets 15-21 with threshold n=5

3.2 Analysis of Doppler statistics

For each individual range bin of the clutter patch the evolution of the Doppler spectrum in slow time (spectrogram) has been calculated using a Short Time Fourier Transform (STFT). This processing used time windows of 256 ms with overlap 50%, 256 bin FFT, and a -55 dB Dolph-Chebyshev window.

Figure 8 shows an example of spectrograms for dataset 6 and corresponding to 105° bistatic angle for different polarizations. The data in the Doppler were selected at the range bin in the middle of the clutter patch where the transmitter and receiver beams intersect. The figures have been normalized so that the peak level in each plot is equal to 0 dB. The clutter Doppler spectrum appears to be localized in the region between 0 Hz and approximately 120 Hz.

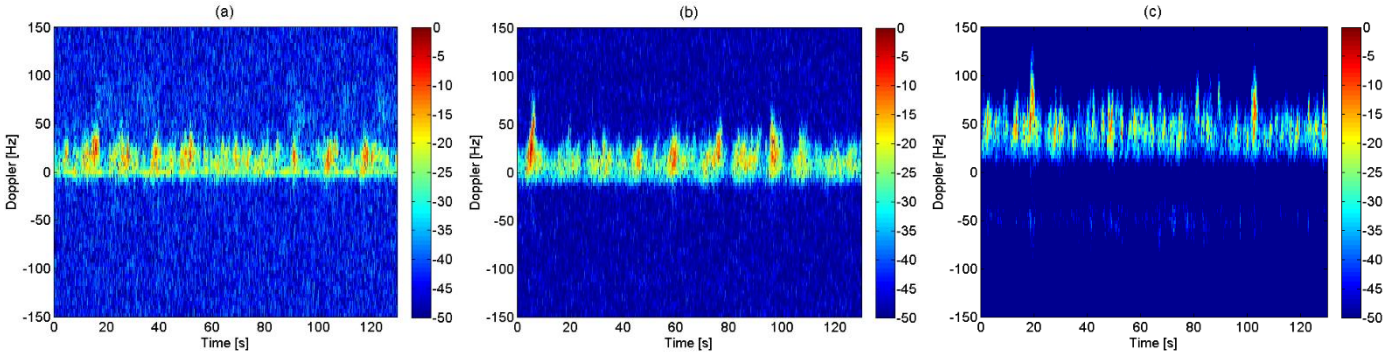

Figure 8 Spectrograms for data collected with bistatic angle β=105° at different polarizations: (a) HH at Bistatic node 1, (b) HV at Bistatic node 2, and (c) HH at Monostatic node 3

The time series of data for each Doppler bin containing clutter were used to estimate the shape parameter of K or K+Noise distributions, depending on the value of the clutter-noise-ratio (CNR). For each dataset the CNR was normalised to the maximum value and compared with thresholds for the time series of data at each range-Doppler cell. If the CNR was within 3 dB from the maximum (which happens in the middle of the internal region of the clutter spectrograms, i.e. endo-clutter) or below 15 dB from the maximum (which happens at noise-limited Doppler bins where there is no clutter, i.e. exo-clutter), the K distribution was used as it was observed that in the former case the effect of the noise was practically negligible when fitting the data, and in the latter case a K distribution with high shape parameter, i.e. a Rayleigh distribution, was suitable. The K+Noise distribution was used in the range-Doppler cells with intermediate range of CNR values where there is a transition between clutter and noise. This process produced a shape parameter value for each Doppler bin of the spectrogram of each range bin included in the clutter patch.

In order to compare the spikiness of monostatic and simultaneous co-polarized and cross-polarized bistatic data in Doppler domain, results can be presented by showing the shape parameter as a function of Doppler shift. Rather than plotting the shape parameter, the inverse value *1/v* has been used to provide a better graphical representation, hence less spiky clutter will be associated to lower values of the inverse shape parameter and more spiky clutter to higher values. Figure 9 shows an example of inverse shape parameter as function of Doppler from data collected with 75° bistatic angle and different polarizations. These results are related to the range bin in the middle of the clutter patch. The monostatic inverse shape parameter has higher values for a wider part of the Doppler spectrum in comparison with both co-polarized and cross-polarized bistatic data, for instance between approximately 50 Hz and 110 Hz for the monostatic case and between approximately 40 Hz and 60 Hz for the bistatic cases in figure 9c. This extends to the Doppler domain the conclusion highlighted in the previous section regarding amplitude statistics, and appears to be in line with previous results with other NetRAD data [5, 6, 33]. The characterization of micro-Doppler signatures of sea clutter, the effect of the sea surface micro-motions as a function of the sea state, and the use of this knowledge for detection of maritime targets, especially those presenting low observability, was also investigated in [38,39].

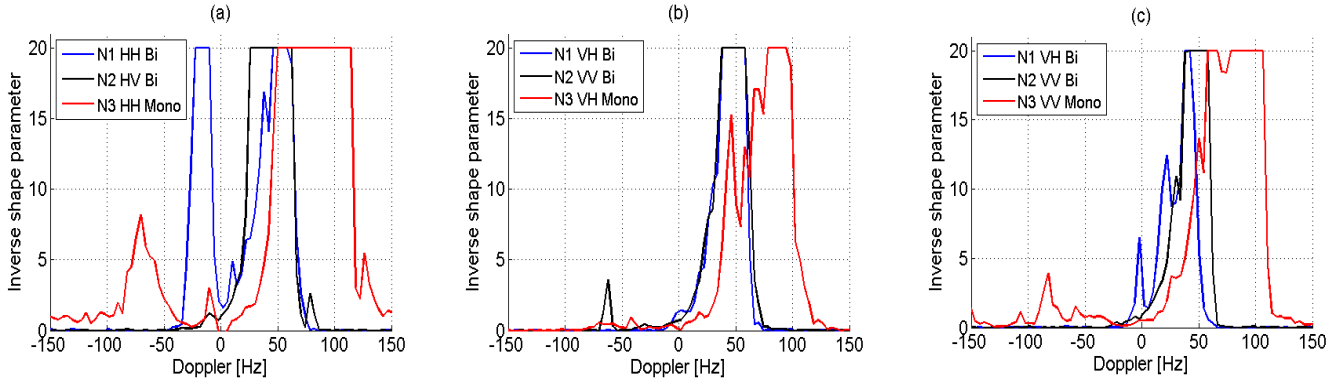

Figure 9 K+Noise inverse shape parameter as function of Doppler for β=75° at different polarizations: (a) dataset 2, (b) dataset 9, and (c) dataset 16

Figure 10 presents the inverse shape parameter values as a function of Doppler and range bins for the dataset collected with 75° bistatic angle and different polarizations. In these figures the monostatic clutter appears to be more spiky over the whole grid of range and Doppler cells in comparison with both co-polarized and cross-polarized bistatic clutter, as the inverse shape parameter is higher. Comparing simultaneous co-polarized and cross-polarized bistatic clutter, it appears that the inverse shape parameter is on average lower for the latter across the whole set of range and Doppler cells, hence the cross-polarized clutter is expected to be less spiky.

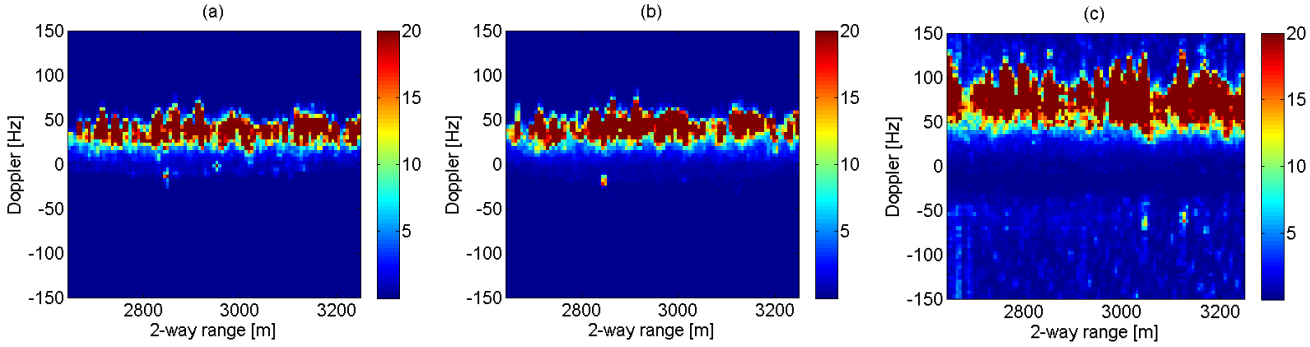

Figure 10 Inverse shape parameter as function of Doppler and range for β=75°: (a) Bistatic node 1 VH pol, (b) Bistatic node 2 VV pol, and (c) Monostatic node 3 VH pol

In order to summarize the analysis of the spikiness of the clutter in the Doppler domain, the number of range Doppler cells with inverse shape parameter values equal or greater than 10 were counted in each range Doppler figure. The results are presented in Table 2 as percentage of these cells over the total number of cells. The percentage of range Doppler cells with spiky clutter is much higher for monostatic data than for both co-polarized and cross-polarized bistatic data, and this trend is observable for all the bistatic angles and polarizations considered in this paper. Comparing the simultaneous co-polarized and cross-polarized bistatic clutter, the percentage of cells with very spiky clutter is consistently higher for the former for both the HH vs HV case (first seven datasets), and tends to be higher for the VV vs VH case (remaining fourteen datasets). These trends in the spikiness of the clutter in the Doppler domain when comparing monostatic vs bistatic and simultaneous bistatic at different polarizations are similar to those observed for amplitude statistics in the

previous section. Figure 11 shows graphically how the bistatic to monostatic ratio of the percentages of range-Doppler cells with inverse shape parameter equal to or greater than 10 changes as a function of bistatic angle. Separate figures for each polarization used at the monostatic node were generated to have a comparison between simultaneous mono vs bi co-pol and bi-cross-pol, rather than comparing measurements taken with the same bistatic angle but separated even hours apart in time. Looking at figure 11a, i.e. for transmitted H polarisation, it appears that the co-polarized bistatic data tends to have higher number of "spiky cells" than the simultaneous cross-polarized with respect to the polarization used at the monostatic node. For transmitted V polarisation as in figures 11b and 11c, the differences in ratio of bistatic to monostatic appear to be smaller. In any cases a strong dependence of these ratios on bistatic angles was observed.

Table 2 Percentage of Range-Doppler cells with values of inverse shape parameter equal or greater than 10 for the available data

Pol TX-RX	Dataset number	Bistatic Angle [°]	Bistatic N1 [%]	Bistatic N2 [%]	Monostatic N3[%]
N3 HH N1 HH N2 HV	1	60	21.52	13.14	36.13
	2	75	12.92	12.92	44.29
	3	85	21.01	10.92	38.86
	4	90	12.15	7.17	29.22
	5	95	12.58	9.30	32.67
	6	105	6.67	6.40	31.56
	7	120	5.99	4.44	25.19
N3 VH N1 VH N2 VV	8	60	10.21	12.36	29.70
	9	75	9.80	12.15	39.48
	10	85	9.30	10.17	29.22
	11	90	7.53	7.80	26.68
	12	95	5.77	5.87	25.07
	13	105	5.87	6.74	21.49
	14	120	2.15	2.87	9.85
N3 VV N1 VH N2 VV	15	60	13.62	11.93	29.39
	16	75	16.37	16.71	34.82
	17	85	7.34	7.90	26.06
	18	90	6.67	7.51	21.64
	19	95	6.69	6.21	19.78
	20	105	3.60	3.57	11.71
	21	120	3.69	5.29	12.22

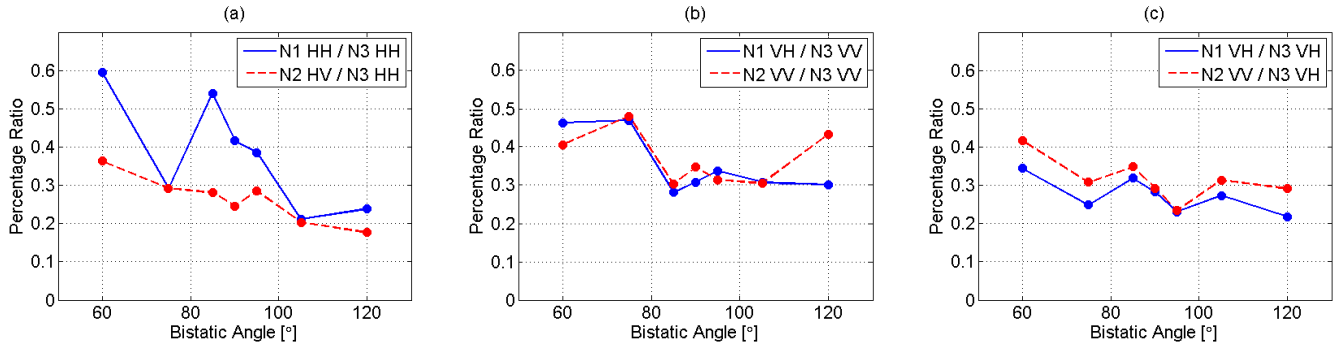

Figure 11 Bistatic to monostatic percentage ratio of Range-Doppler cells with values of inverse shape parameter equal to 10 as function of bistatic angle β: (a) HH pol at monostatic node, (b) VV pol at monostatic node, and (c) VH pol at monostatic node

3.3 Examples of correlation analysis

The temporal and spatial correlation were evaluated for a couple of key datasets, example of results of these are presented here. Figure 12 shows the temporal correlation for datasets 3 and 17 from Table 1, which have transmitted H polarisation and V polarisation respectively, in both cases with bistatic angle equal to 85°. The temporal correlation of the clutter was evaluated as the cross-covariance, which is defined as the auto-correlation of the data minus the mean of the samples, defined below.

$$c_x(m) = \frac{1}{N}\sum_{n=0}^{N-m-1}\left[(x_{n+m} - \frac{1}{N}\sum_{i=0}^{N-1} x_i)(x_n^* - \frac{1}{N}\sum_{i=0}^{N-1} x_i^*)\right] \quad (7)$$

Where c_x is the covariance, x is the data, N is the number of samples and m is the lag of the covariance. This was evaluated for each range gate over a number of time 200 lags, equal to 0.2 seconds. The mean covariance has then been generated to show a direct comparison between the simultaneous data from all three nodes.

The decorrelation time for each dataset was then extracted from the mean covariance curve. This decorrelation time is defined as the time for the temporal ACF to cross below the threshold value of 1/*exp*(1). This was found to be equal to 77 ms, 67 ms, and 123 ms, respectively for node 1 (bistatic node), node 2 (bistatic node), and node 3 (monostatic node) for the results shown in Fig 12a. Which shows that the monostatic decorrelation time was approximately double the simultaneous bistatic result for HH transmitted polarisation. For the results shown in Fig 12b the decorrelation times are equal to 71 ms (bistatic node 1), 88 ms (bistatic node 2), and 73 ms (monostatic node 3). Demonstrating a much closer value for all three nodes for the VV polarisation transit data.

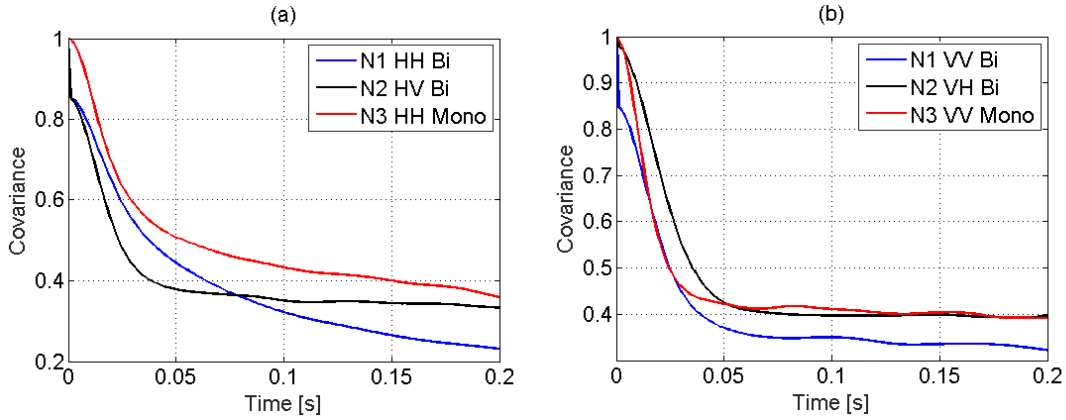

Figure 12 Temporal ACF: (a) Dataset 3 with transmitted H polarisation, and (b) Dataset 17 with transmitted V polarisation

The spatial correlation of the same two example datasets was calculated for comparison. In order to evaluate the spatial correlation samples from all range gates were extracted from pulses separated by the decorrelation time, from the prior analysis above, in order to remove speckle contribution from the spatial correlation. A group of 32 of these selected pulses were summed and input to the covariance calculation, in order to take an average of this subset. The covariance was evaluated over lags equal to the full number of range bins for each selected clutter patch within the dataset. This process was repeated across all pulses within a dataset and the average covariance values have been plotted in Fig. 13.

The results show that the spatial correlation of the monostatic data in both cases was relatively flat over the ranges shown. In comparison both bistatic nodes (node 1 and 2) showed sinusoidal correlations over long range sections (>200 m) in dataset 17 and for the bistatic node 2 in dataset 3. There is very little analysis of the spatial correlation of simultaneous monostatic and bistatic data and these initial results show key example profiles. Further comprehensive analysis of this behaviour and the development of models for this is considered as important future work for sea clutter analysis.

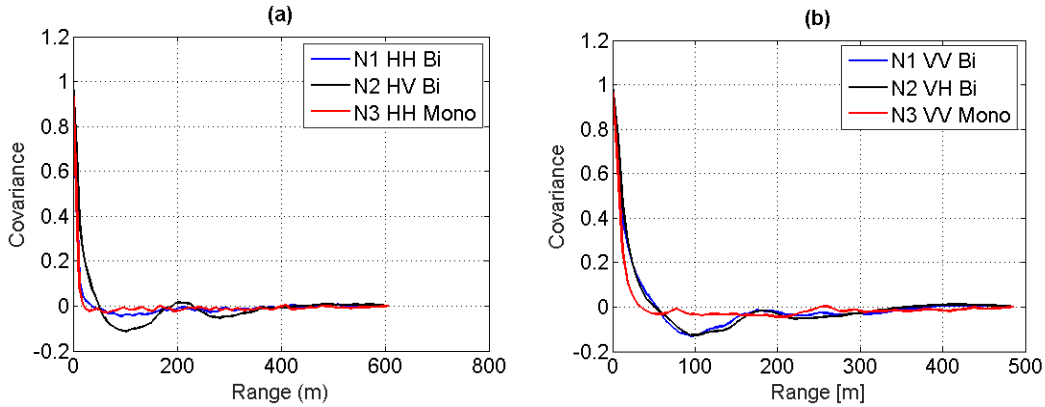

Figure 13 Spatial correlation: (a) Dataset 3 with transmitted H polarisation, and (b) Dataset 17 with transmitted V polarisation

4. Conclusions

In this paper a comparative analysis of simultaneous monostatic and bistatic low grazing angle S-band clutter has been presented. These data were collected in 2011 and we have not found any report of data of this kind in the literature, as they include simultaneous monostatic and co-polarized and cross-polarized bistatic recordings, allowing a direct comparison of their characteristics across a range of different bistatic angles from 60° to 120°. The analysis has focused on fitting the data to the K+Noise distribution and on evaluating the shape parameter as a function of range and Doppler for different bistatic angles and polarizations in order to characterize the spikiness of the clutter. It has been shown that bistatic clutter can be less spiky than the simultaneous monostatic clutter in range and Doppler domain, and that cross-polarized bistatic clutter tends to be also less spiky than the simultaneous co-polarized clutter. These results help better understand the "clutter diversity", i.e. the variation of sea clutter characteristics as a function of numerous parameters, such as bistatic angles and polarizations, in order to design and deploy more effective bistatic radar systems and implement detection algorithms for low observable maritime targets such as small boats or submarine periscopes. The analysis of the K+noise shape parameters seems to suggest that at bistatic angles around 90° the clutter appears to be less spiky at all polarizations (i.e. higher value of shape parameter), hence more favourable for detection.

Further work on these data can improve the understanding of bistatic clutter behaviour. Different distributions that provide better models for non-Rayleigh sea spikes (e.g. KA and KK distribution) can be fitted to the data to extend the comparison monostatic vs co-polarized and cross-polarized bistatic. Specific analysis of sea spike properties such as amplitude, duration, and temporal interval between spikes may be performed in a similar way as in [35, 37] to extend the preliminary analysis of spikes performed in section 3. A more detailed analysis of the spatial and temporal correlation properties of the clutter in these data can be also performed, highlighting trends as a function of bistatic angles and polarisations. Although the main aim of this paper was to get to the attention of the research community and literature these data and the related trends, further work in theoretical and electromagnetic analysis could be combined with the experimental approach used here in order to gain a more comprehensive understanding and characterization of the phenomena.

The data collection processing will be improved in the radar system NeXtRAD, the successor of NetRAD, where telescopic mounts for automatic antenna steering will be used, as well as videos recording to monitor the environmental conditions for each measurement [40]. This will provide reliable ground truth for the data in terms of wind speed and direction and wave height and direction together with each measurement, as well as time-stamped images of the sea surface to correlate back to the data. The electronic alignment of the antennas will reduce possible misalignment errors that may have occurred when using the telescopic sights and the Vernier scale.

Acknowledgement

The authors would like to thank the rest of the team from the University of Cape Town who collected the data. The development of the NetRAD system and the experimental campaign were funded by the UK Engineering and Physical Sciences Research Council (EPSRC), THALES UK, THALES NL, Royal Academy of Engineering, and the Office of Naval Research Global (ONR-G). The UCT contribution to the radar development and trials was funded by the South African National Defence Force Project Ledger through student bursaries. Dr F. Fioranelli and Dr M. Ritchie are supported by the IET A F Harvey Prize 2013 awarded to Prof H. Griffiths.

The authors would like to thank the reviewers for their suggestions and comments to improve the paper.

References

[1] N. J. Willis and H. Griffiths, *Advances in Bistatic Radar*, SciTech Publishing, 2007, Raleigh, NC.

[2] T. E. Derham, S. Doughty, K. Woodbridge, and C. J. Baker, 'Design and evaluation of a low-cost multistatic netted radar system', *IET Radar, Sonar & Navigation,* vol. 1, pp. 362-368, 2007.

[3] W. A. Al-Ashwal, K. Woodbridge, and H. D. Griffiths, 'Analysis of bistatic sea clutter Part I: average reflectivity', *IEEE Transactions on Aerospace and Electronic Systems,* vol. 50, pp. 1283-1292, 2014.

[4] W. A. Al-Ashwal, K. Woodbridge, and H. D. Griffiths, 'Analysis of bistatic sea clutter Part II: amplitude statistics', *IEEE Transactions on Aerospace and Electronic Systems,* vol. 50, pp. 1293-1303, 2014.

[5] M. A. Ritchie, W. A. Al-Ashwal, A. G. Stove, K. Woodbridge, and H. D. Griffiths, 'Statistical analysis of monostatic and bistatic sea clutter Doppler spectrum,' *CIE 2011 International Radar Conference,* pp. 816-820, October 24-27, Chengdu.

[6] M. A. Ritchie, W. A. Al-Ashwal, A. G. Stove, K. Woodbridge, and H. D. Griffiths, 'Coherent analysis of horizontally-polarized monostatic and bistatic sea clutter,' *IET 2012 International Conference on Radar Systems,* pp. 1-5, October 22-25, Glasgow.

[7] W. A. Al-Ashwal, C. J. Baker, A. Balleri, H. D. Griffiths, R. Harmanny, M. Inggs, *et al.*, 'Statistical analysis of simultaneous monostatic and bistatic sea clutter at low grazing angles,' *Electronics Letters,* vol. 47, pp. 621-622, 2011.

[8] V. Pidgeon, 'Bistatic cross section of the sea,' *IEEE Transactions on Antennas and Propagation,* vol. 14, pp. 405-406, 1966.

[9] T. P. Kochanski, M. J. Vanderhill, J. V. Zolotarevsky, and T. Fariss, 'Low illumination angle bistatic sea clutter measurements at X-band,' *Proceedings of OCEANS '92.*, pp. 518-523, October 26-29, Newport, Rhode Island.

[10] W.A.Al-Ashwal, 'Measurement and modelling of bistatic sea clutter,' Ph.D. Dissertation, University College London, UK, 2011.

[11] J. S. Sandenbergh, M. R. Inggs, and W.A.Al-Ashwal, 'Evaluation of coherent netted radar carrier stability while synchronised with GPS-disciplined oscillators', *2011 IEEE Radar Conference*, pp. 1100-1105, May 23-27, Kansas City.

[12] J. S. Sandenbergh and M. R. Inggs, 'A common view GPSDO to synchronize netted radar,' *IET 2007 International Conference on Radar Systems*, pp. 1-5, Oct 15-18, Edinburgh.

[13] E. Jakeman and P. N. Pusey, 'A model for non-Rayleigh sea echo,' *IEEE Transactions on Antennas and Propagation*, vol. 24, pp. 806-814, 1976.

[14] K. D. Ward, 'Compound representation of high resolution sea clutter,' *Electronics Letters*, vol. 17, pp. 561-563, 1981.

[15] K. Ward, R. Tough, and S. Watts, *Sea Clutter: Scattering, the K Distribution and Radar Performance, 2nd Edition*: Institution of Engineering and Technology, 2013, Stevenage, UK.

[16] G. V. Trunk and S. F. George, 'Detection of targets in non-Gaussian sea clutter,' *IEEE Transactions on Aerospace and Electronic Systems, v*ol. AES-6, pp. 620-628, 1970.

[17] D. C. Schleher, 'Radar detection in Weibull clutter,' *IEEE Transactions on Aerospace and Electronic Systems*, vol. AES-12, pp. 736-743, 1976.

[18] M. Greco, F. Bordoni, and F. Gini, 'X-band sea-clutter nonstationarity: influence of long waves,' *IEEE Journal of Oceanic Engineering*, vol. 29, pp. 269-283, 2004.

[19] G. V. Weinberg, 'Assessing Pareto fit to high-resolution high-grazing-angle sea clutter,' *Electronics Letters*, vol. 47, pp. 516-517, 2011.

[20] M. Farshchian and F. L. Posner, 'The Pareto distribution for low grazing angle and high resolution X-band sea clutter,' *2010 IEEE Radar Conference*, pp. 789-793,May 10-14, Washington.

[21] K.J. Sangston, F. Gini, M. Greco, 'Coherent Radar Target Detection in Heavy-Tailed Compound-Gaussian Clutter', *IEEE Transactions on Aerospace and Electronic Systems*, vol. 48 (1), pp. 64-77, 2012.

[22] S. Watts, 'Radar detection prediction in K-distributed sea clutter and thermal noise,' *IEEE Transactions on Aerospace and Electronic Systems*, vol. AES-23, pp. 40-45, 1987.

[23] A. Farina, F. Gini, M. Greco, L. Verrazzani, 'High resolution sea clutter data: statistical analysis of recorded live data', *IEE Proceeedings Radar, Sonar and Navigation*, vol. 144 (3), pp. 121-130, 1997.

[24] D. Middleton, 'New physical-statistical methods and models for clutter and reverberation: the KA-distribution and related probability structures,' *IEEE Journal of Oceanic Engineering*, vol. 24, pp. 261-284, 1999.

[25] K. D. Ward and R. J. A. Tough, 'Radar detection performance in sea clutter with discrete spikes,' *2002 IEEE RADAR Conference*, pp. 253-257, April 22-25, Long Beach, California.

[26] L. Rosenberg, D. J. Crisp, and N. J. Stacy, 'Analysis of the KK-distribution with medium grazing angle sea-clutter,' *IET Radar, Sonar & Navigation,* vol. 4, pp. 209-222, 2010.

[27] E. Conte, A. De Maio, C. Galdi, 'Statistical analysis of real clutter at different range resolutions', *IEEE Transactions on Aerospace and Electronic Systems*, vol. 40 (3), pp. 903-918, 2004.

[28] E. Conte, M. Lops, G. Ricci, 'Adaptive detection schemes in compound Gaussian clutter', *IEEE Transactions on Aerospace and Electronic Systems*, vol. 34 (4), pp.1058-1069, 1998.

[29] M. Sahed, A. Mezache, T. Laroussi, 'A novel [zlog(z)] based closed form approach to parameter estimation of k-distributed clutter plus noise for radar detection', *IEEE Transactions on Aerospace and Electronic Systems*, vol. 51 (1), pp. 492-505, 2015.

[30] D. Blacknell, R. Tough, 'Parameter estimation for the K-distribution based on [zlog(z)]', *IEE Proceeedings Radar, Sonar and Navigation*, vol. 148 (6), pp. 309-312, 2001.

[31] S. Bocquet, 'Parameter estimation for Pareto and K distributed clutter with noise', *IET Radar, Sonar & Navigation*, vol. 9 (1), pp. 104-113, 2015.

[32] W. A. Al-Ashwal, A. Balleri, H. D. Griffiths, W. J. Miceli, K. Woodbridge, C. J. Baker, *et al.*, 'Measurements of bistatic radar sea clutter,' *2011 IEEE Radar Conference*, pp. 217-221, Kansas City, MO, May 23-27.

[33] R. Palamà, M. Greco, P. Stinco, F. Gini, 'Analysis of sea spikes in NetRAD clutter', *2014 EuRAD European Radar Conference*, Rome, Italy, October 5-10.

[34] R. Palamà, M. Greco, P. Stinco, F. Gini, 'Statistical analysis of bistatic and monostatic sea clutter', *IEEE Transactions on Aerospace and Electronic Systems*, vol. 51 (4), pp. 64-77, 2015.

[35] L. Rosenberg, 'Sea-spike detection in high grazing angle X-band sea-clutter,' *IEEE Transactions onGeoscience and Remote Sensing*, vol. 51, pp. 4556-4562, 2013.

[36] H. W. Melief, H. Greidanus, P. Van Genderen, and P. Hoogeboom, 'Analysis of sea spikes in radar sea clutter data,' *IEEE Transactions on Geoscience and Remote Sensing*, vol. 44, pp. 985-993, 2006.

[37] M. Greco, P. Stinco, and F. Gini, 'Identification and analysis of sea radar clutter spikes,' *IET Radar, Sonar & Navigation,* vol. 4, pp. 239-250, 2010.

[38] X. Chen, J. Guan, Z. Bao, and Y. He, 'Detection and extraction of target with micromotion in spiky sea clutter via short-time fractional Fourier transform', *IEEE Transactions on Geoscience and Remote Sensing,* vol. 52, pp. 1002-1018, 2014.

[39] X. Chen, J. Guan, X. Li, and Y. He, 'Effective coherent integration method for marine target with micromotion via phase differentiation and radon-Lv's distribution', *IET Radar, Sonar & Navigation,* vol. 9, pp. 1284-1295, 2015.

[40] M. Inggs, H. Griffiths, F. Fioranelli, M. Ritchie, and K. Woodbridge, 'Multistatic radar: System requirements and experimental validation', *SEE 2014 International Radar Conference*, pp. 1-6, Lille, France, October 13-17.